J. Rubb. Res., 4(4), 222–244

Non-linear Hysteresis Models for Ultra-high Damping NR Structural Dampers

RICHARD SAUSE*#, KYUNG-SIK LEE*, JAMES RICLES*,
KAMARUDIN AB-MALEK** AND LE-WU LU*

Models for ultra-high damping natural rubber (UHDNR), a new material for structural dampers, are investigated. Experimental tests of structural dampers made from UHDNR and the observed mechanical properties are summarised. Two load rate independent hysteresis models, which are more accurate for UHDNR than existing hysteresis models, are proposed. Good agreement is observed between the experimental results and the models. The more complex of the two models, the sequential asymptote model, represents accurately the behaviour of UHDNR under the random load histories that are anticipated for structural dampers.

Key words: Non-linear; hysteresis; model; ultra-high damping; NR; structural dampers; mechanical properties; random load

Structural dampers are passive energy dissipation devices used to protect structures from dynamic loads such as earthquake and wind. Structural dampers absorb and dissipate input energy through inelastic deformation, and, as a result, the response of the structure is decreased. Several types of structural dampers, including steel yielding, friction, viscoelastic, viscous fluid, and tuned mass dampers, have been developed and used in buildings and bridges during the past four decades. This study focuses on ultra high damping natural rubber (UHDNR) dampers.

The use of rubber for earthquake protection of structures has a 20-year history. High damping rubber (HDR), with an equivalent damping ratio of approximately 10%, has been used in base isolators for buildings and bridges. It is well known that HDR exhibits non-linear behaviour that depends on strain amplitude, loading frequency, temperature, and loading history. Numerous experimental and analytical studies of the behaviour of HDR isolators under simulated earthquake loading have been conducted (see, for example[1,3–5]). Models for the non-linear behaviour of HDR have focused on the strain dependence of HDR. Strain amplitudes up to 300% have been considered in these models. A base isolator is typically located at the foundation of a structure, and much of the lateral displacement of the structure under earthquake loading is designed to take place at the foundation level, resulting

* Department of Civil and Environmental Engr., ATLSS Center, Leheigh University, Bethlehem, PA 18015, USA
** Rubber Research Institute of Malaysia, Malaysian Rubber Board, P. O. Box 10150, 50908 Kuala Lumpur, Malaysia
# Corresponding author (e-mail: rs0c@lehigh.edu)

in large strain demands on the isolator. Structural dampers are usually located within the structure, and are subjected to much smaller strains, up to perhaps 100%. Generally, structural dampers require an equivalent damping ratio significantly greater than 10%.

To investigate the potential for ultra-high damping natural rubber (UHDNR) structural dampers, experimental tests of prototype UHDNR structural dampers and analytical studies of structures with UHDNR dampers are needed. This paper summarises data from experiments on prototype UHDNR dampers and presents hysteresis models which can accurately predict the behaviour of UHDNR dampers for strains up to 100%. The models are intended for use in dynamic time history simulations of structures with UHDNR dampers under earthquake loading[7].

EXPERIMENTAL TESTS

The mechanical properties of structural dampers made from a newly-developed UHDNR have been studied through a series of experiments conducted at the ATLSS Center at Lehigh University. The structural dampers, shown in *Figure 1*, consist of two layers of UHDNR material bonded between three steel plates. When the forces are applied in the axial direction of the plates, the layers of UHDNR deform in shear. The dampers were fabricated at the Malaysian Rubber Board and the properties of the UHDNR compound which was cured at 145°C for 30 min are shown in *Table 1*.

During the experiments, a series of constant amplitude sinusoidal displacement histories were applied to the dampers, resulting in sinusoidal shear strain histories in the UHDNR layers. Each displacement history was selected to produce a shear strain amplitude in the UHDNR layers between 20% and 100%. The displacement histories were applied using a MTS 810 Material Test System[8], and two external displacement transducers were used to verify the displacement histories. The shear strain history at each strain amplitude consisted of ten complete cycles at a frequency of 0.5 Hz. The ambient temperature for these experiments was held constant at 20°C. Experiments at other frequencies and ambient temperatures

TABLE 1. PROPERTIES OF UHDNR COMPOUND

Tensile strength, unaged (*ISO 37*) (MPa)	6.6
Tensile strength, aged (*ISO 37*) 7 days/70° C (MPa)	7.1
Elongation at break, unaged (*ISO 37*) (%)	300
Elongation at break, aged (*ISO 37*) 7 days/70° C (%)	330
Tensile modulus at 100%, unaged (*ISO 37*) (MPa)	2.2
Tensile modulus at 100%, aged (*ISO 37*) (MPa)	2.5
Hardness, unaged (*ISO 48*) (IRHD)	87
Hardness, aged (*ISO 48*) (IRHD)	96
Compression set @ 24 h/70° C	66.7
Trouser tear, unaged (*ISO 34*) (N/mm)	6

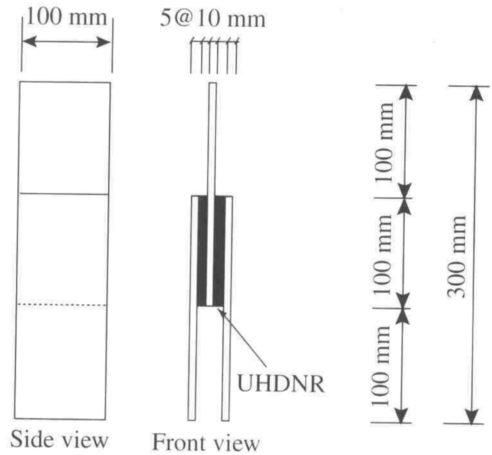

(a) Configuration of structural Damper made from UHDNR

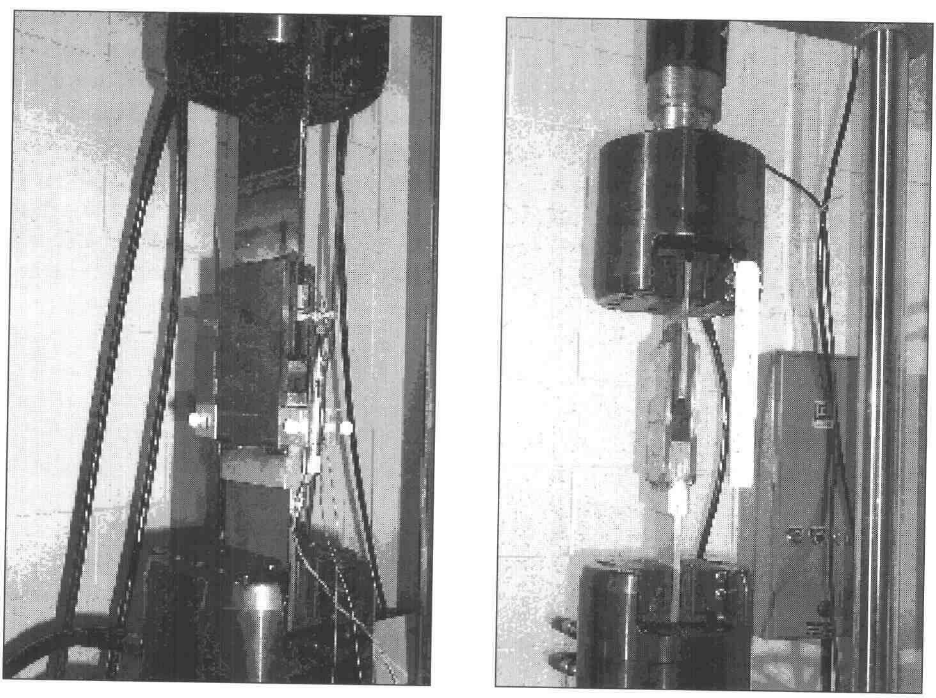

(b) Experimental test set-up

Figure 1. Configuration of structural damper made from UHDNR and experimental test set-up.

were conducted and are summarised by Lee[7].

Figure 2 shows a typical shear stress-strain hysteresis loop obtained from a UHDNR damper experiment where the amplitude of the sinusoidal shear strain history is 100%. *Figure 2* shows that the hysteresis loops are repeatable. Significant stiffness degradation was not observed within the ten-cycle history, although the first two cycles have slightly higher stiffness than the subsequent cycles. Filled rubbers often have a higher stiffness in the first cycle of loading than in subsequent cycles. A decrease in stiffness, known as Mullin's effect[9], occurs over a few cycles of loading and the hysteresis loops stabilise thereafter.

The equivalent shear modulus and loss factor are often used to define the mechanical properties of damping materials. The equivalent shear modulus, G_{eq}, shown in *Figure 3* is defined as the ratio of the maximum stress to the maximum strain. To define the equivalent loss factor, the material is treated as a linear viscoelastic material with an elastic shear modulus of G', a loss factor of $\tan(\delta)$, and a complex shear modulus amplitude of $G^* = G'[1+[\tan(\delta)]^2]^{1/2}$ equal to G_{eq}.

For a linear viscoelastic material, the loss factor is:

$$\tan(\delta) = \frac{ED}{2\pi\, ES} \qquad \ldots 1$$

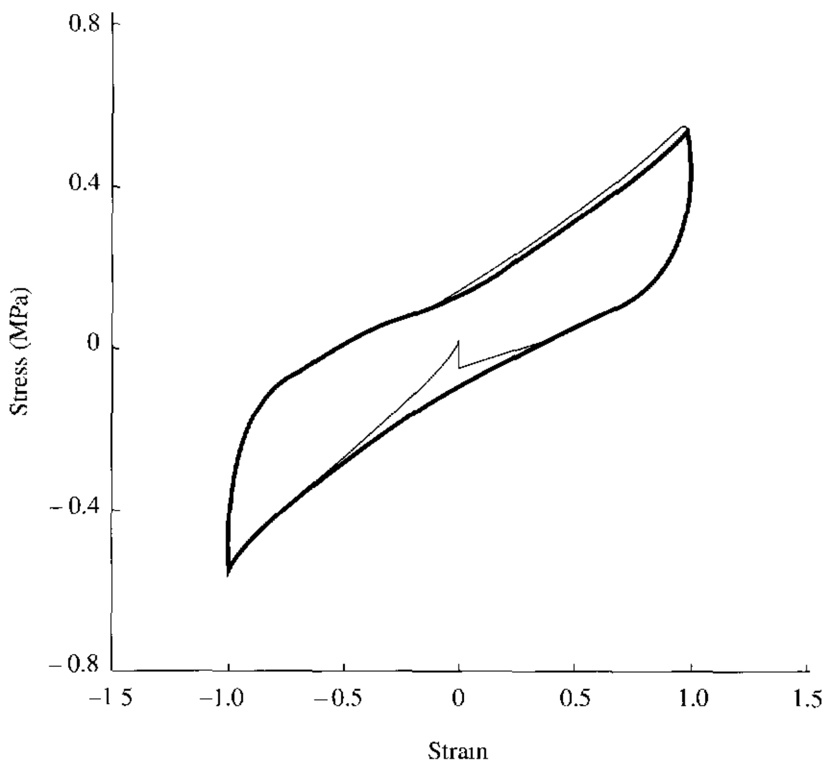

Figure 2. Typical hysteresis loops of UHDNR.

where, *ED* is the energy dissipated per cycle of sinusoidal loading, and *ES* is the maximum strain energy stored in a cycle of sinusoidal loading. In *Equation 1*, the energy dissipated, *ED*, can be calculated directly by integrating the hystersis loops, as shown in *Figure 3*. The maximum strain energy stored, *ES*, is not easily calculated from the hysteresis loops, however, *ES* can be defined in terms of the elastic shear modulus, *G'*, and the equivalent shear modulus, G_{eq}, as follows:

$$ES = \frac{1}{2} G' \gamma^2_{max} = \frac{1}{2} \frac{G_{eq}}{2\sqrt{1+[\tan(\delta)]^2}} \gamma^2_{max} \quad \ldots 2$$

where: γ_{max} is the shear strain amplitude in the cycle of sinusoidal loading. Substituting *Equation 2* into *Equation 1*, and using the trigonometric rule $\sin(\delta) = \tan(\delta)/[1+[\tan(\delta)]^2]^{1/2}$ results in the following:

$$\sin(\delta) = \frac{ED}{\pi G_{eq} \gamma^2_{max}} \quad \ldots 3$$

With *ED* calculated from the shear stress-strain hysteresis loop, *Equation 3* can be used to determine $\sin(\delta)$, and the equivalent loss factor is $\tan(\delta)_{eq} = \sin(\delta)/\{1-[\sin(\delta)]^2\}^{1/2}$. The equivalent stiffness, G_{eq}, and equivalent loss factor, $\tan(\delta)_{eq}$, from the UHDNR structural damper experiments are given in *Table 2*. These values are averages of results for cycles 4,5,6, and 7 of each ten-cycle sinusoidal shear strain history. $\tan(\delta)_{eq}$ for UHDNR structural dampers is quite high, about 0.35 to 0.40. It is observed that G_{eq}

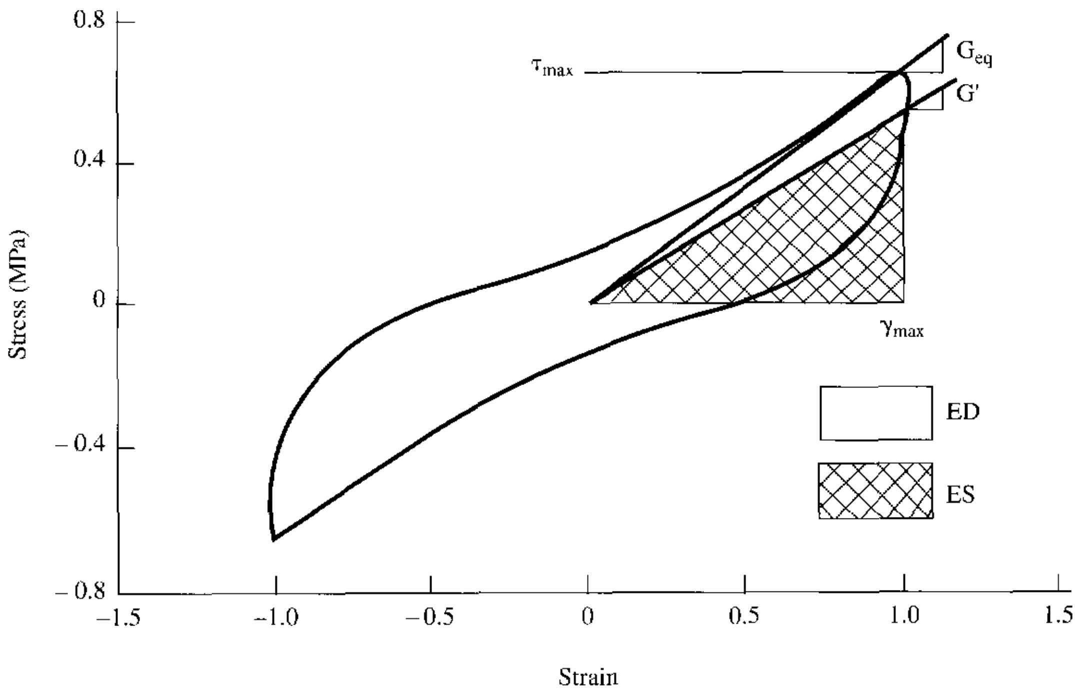

Figure 3. Definition of equivalent shear modulus, energy dissipated, and energy stored.

TABLE 2. MECHANICAL PROPERTIES EVALUATED FROM THE EXPERIMENTAL TESTS

Strain amplitude (%)	G_{eq}(MPa)	$\tan(\delta)_{eq}$
20	0.782	0.411
30	0.684	0.394
40	0.627	0.383
50	0.588	0.374
60	0.559	0.369
70	0.540	0.363
80	0.528	0.356
90	0.526	0.346
100	0.531	0.334

and $\tan(\delta)_{eq}$ gradually decrease with increasing strain amplitude.

HYSTERESIS MODELS

HDR materials exhibit highly non-linear stress-strain behaviour, including strain, frequency, and temperature dependence under cyclic loading[10]. In the current paper, only strain dependence is considered in models of the stress-strain behaviour, because this is the dominant factor. Attention is limited to the typical range of load frequency and temperature for buildings.

Rate-independent differential models, such as the Bouc-Wen model[11] and the Ahmadi model[1] have been widely used in the analysis of base isolation systems. The current models[1,5] have been developed for strains up to 300% (appropriate for base isolators). This paper focuses on hysteresis models for UHDNR that are accurate for strains up to 100%.

Ahmadi *et al.*[1] presented a differential hysteresis model for HDR, based on the stress-strain behaviour of HDR in simple shear tests, as follows:

$$\frac{d\tau}{d\gamma} = \frac{d\bar{\tau}(\gamma)}{d\gamma}\left[1 + k_1\frac{e}{e_0}\right] + k_2\left|\frac{d\tau_1(\gamma)}{d\gamma} - \frac{d\tau_2(\gamma)}{d\gamma}\right|\frac{e}{e_0} \quad \ldots 4$$

where, (γ) indicates a function of γ; $\tau_1(\gamma)$ and $\tau_2(\gamma)$ are the asymptotes for the loading (positive increment of strain, γ) direction and the unloading (negative increment of strain, γ) direction, respectively; $\bar{\tau}(\gamma)$ is the target asymptote, either $\tau_1(\gamma)$ or $\tau_2(\gamma)$ depending on the loading direction; e is the stress deviation between $\bar{\tau}(\gamma)$ and the current stress,$\tau(\gamma)$; e_0 is the stress deviation between $\bar{\tau}(\gamma)$ and the stress at the most recent strain reversal (change in loading direction), $\tau_0(\gamma)$; and k_1 and k_2 are constants. The first term on the right side of *Equation 4* captures the softening that occurs for shear strains up to 100%, and the second term in the right side of *Equation 4* captures the stiffening that occurs for shear strains greater than 300%. After any strain reversal, the target asymptote, $\bar{\tau}(\gamma)$, and the stress deviation, e_0, are established and the stress-strain path (until the next strain reversal) is uniquely described by *Equation 4*. The stress-strain path depends on the stress and strain at the strain reversal, and the parameters k_1 and k_2, and the asymptote functions $\tau_1(\gamma)$, and $\tau_2(\gamma)$ which are established from test data. *Equation 4* was found to be unsuitable for UHDNR considering strains up to 100%, however, several models building on the underlying concepts of *Equation 4* have been developed and are presented below.

Linear Asymptote Model (LAM)

For strains up to 100%, *Equation 4* can be simplified as follows:

$$\frac{d\tau}{d\gamma} = \frac{d\bar{\tau}(\gamma)}{d\gamma}\left[1 + k\frac{e}{e_0}\right] \qquad \ldots 5$$

where, $\bar{\tau}(\gamma)$ is the target asymptote $[\tau_1(\gamma)$ or $\tau_2(\gamma)]$;

$\tau_1(\gamma)$ and $\tau_2(\gamma)$ are asymptote functions, established from experimental data;

$e = \bar{\tau}(\gamma) - \tau(\gamma)$;

$e_0 = \bar{\tau}(\gamma_0) - \tau_0$;

γ_0 and τ_0 are the strain and stress at a strain reversal point; and

k is a material parameter established from experimental data.

A previous study of HDR[1] suggests that, for strains less than 100%, the asymptotes can be assumed linear, that is, $\tau_1(\gamma) = A_1\gamma + A_2$ and $\tau_2(\gamma) = A_1\gamma - A_2$, and then *Equation 5* is as follows:

$$\frac{d\tau}{d\gamma} = \frac{d\bar{\tau}(\gamma)}{d\gamma}\left[1 + k\frac{e}{e_0}\right] = A_1\left[1 + k\frac{e}{e_0}\right] \qquad \ldots 6$$

where, $\bar{\tau}(\gamma)$, e, e_0, γ_0, τ_0, and k are as defined for *Equation 5*, and A_1 and A_2 are material parameters.

The solution to *Equation 6* is a simple closed-form expression for $\tau(\gamma)$:

$$\tau(\gamma) = \bar{\tau}(\gamma) - e_0\,\mathrm{EXP}\left(\frac{A_1 k[\gamma_0 - \gamma]}{e_0}\right) \qquad \ldots 7$$

The right side of *Equation 7* includes two terms. The first term, $\bar{\tau}(\gamma)$, is the target asymptote, and the second term is the difference between $\tau(\gamma)$ and $\bar{\tau}(\gamma)$, which decays as the magnitude of $[\gamma_0 - \gamma]$ increases. As the second term decays, the stress-strain path approaches asymptotically the target asymptote. Values for the material parameters, A_1, A_2, and k, are determined from non-linear regression using the experimental data summarised earlier. The regression procedure is discussed later in the paper. The values for A_1, A_2, and k are given in *Table 3*. Analytical hysteresis loops, generated using *Equation 7* with these parameter values, are compared with experimental hysteresis loops in *Figure 4*. The analytical and experimental results in *Figure 4* are not in acceptable agreement, and the linear asymptote model was not considered further.

Fourth Order Polynomial Asymptote Model (FPAM)

Models with other polynomial asymptotes were studied. Second, third, fourth, and fifth

TABLE 3. PARAMETERS DETERMINED FROM THE NON-LINEAR REGRESSION

Strain	A_1 (MPa)	A_2 (MPa)	A_3 (MPa)	A_4 (MPa)	A_5 (MPa)	k	N
LAM	0.395	0.0985	–	–	–	17.9	–
FPAM	−0.196	0.0951	0.212	0.314	0.0874	11.4	–
FPAPM	−0.182	0.104	0.191	0.293	0.114	18.2	2

order polynomials were investigated, and, ultimately, fourth order polynomial asymptotes were selected: $\tau_1(\gamma)=A_1\gamma^4+A_2\gamma^3+A_3\gamma^2+A_4\gamma+A_5$; and $\tau_2(\gamma)=A_1\gamma^4+A_2\gamma^3+A_3\gamma^2+A_4\gamma-A_5$. With these asymptote functions, *Equation 5* is as follows:

$$\frac{d\tau}{d\gamma} = \frac{d\bar{\tau}(\gamma)}{d\gamma}\left[1 + k\frac{e}{e_0}\right] \quad \ldots 8$$

where, $\dfrac{d\bar{\tau}(\gamma)}{d\gamma} = \dfrac{d\tau_1(\gamma)}{d\gamma}$

$$= 4A_1\gamma^3 + 3A_2\gamma^2 + 2A_3\gamma + A_4$$

for loading; and

$$\frac{d\bar{\tau}(\gamma)}{d\gamma} = \frac{d\tau_2(\gamma)}{d\gamma}$$

$$= -4A_1\gamma^3 + 3A_2\gamma^2 - 2A_3\gamma + A_4$$

for unloading.

e, e_0, γ_0, τ_0, and k are as defined for *Equation 5*, and A_1, A_2, A_3, A_4, and A_5 are material parameters. The solution to *Equation 8* provides the following closed-form expression for $\tau(\gamma)$:

$$\tau(\gamma) = d\bar{\tau}(\gamma) - e_0\,\mathrm{EXP}\left(\frac{\overline{W}(\gamma)\,k[\gamma_0-\gamma]}{e_0}\right) \quad \ldots 9$$

where, for the loading direction,

$\bar{\tau}(\gamma) = \tau_1(\gamma) = A_1\gamma^4+A_2\gamma^3+A_3\gamma^2+A_4\gamma+A_5$; and

$\overline{W}(\gamma) = W_1(\gamma) = A_1[\gamma^3+\gamma^2\gamma_0+\gamma\gamma_0^2+\gamma_0^3]+A_2[\gamma^2+\gamma\gamma_0+\gamma_0^2]+A_3[\gamma+\gamma_0]+A_4$; and for the unloading direction,

$\bar{\tau}(\gamma) = \tau_2(\gamma) = -A_1\gamma^4+A_2\gamma^3-A_3\gamma^2+A_4\gamma-A_5$; and

$\overline{W}(\gamma) = W_2(\gamma) = A_1[\gamma^3+\gamma^2\gamma_0+\gamma\gamma_0^2+\gamma_0^3]+A_2[\gamma^2+\gamma\gamma_0+\gamma_0^2]-A_3[\gamma+\gamma_0]+A_4$.

Values of the material parameters, A_1, A_2, A_3, A_4, A_5, and k, determined from non-linear regression are given in *Table 2*. Analytical hysteresis loops, generated using *Equation 9* with these parameter values, are compared with experimental hysteresis loops in *Figure 5*. Compared to the results shown in *Figure 4* for the linear asymptote model, the results in *Figure 5* show the fourth order polynomial asymptote model is significantly more accurate. The equivalent shear modulus, G_{eq}, and the equivalent loss factor, $\tan(\delta)_{eq}$, are in good agreement, especially for strains between 50% and 100%. However, for hysteresis loops with strain amplitude between 40% and 80%, the stiffness of the analytical stress-strain path after

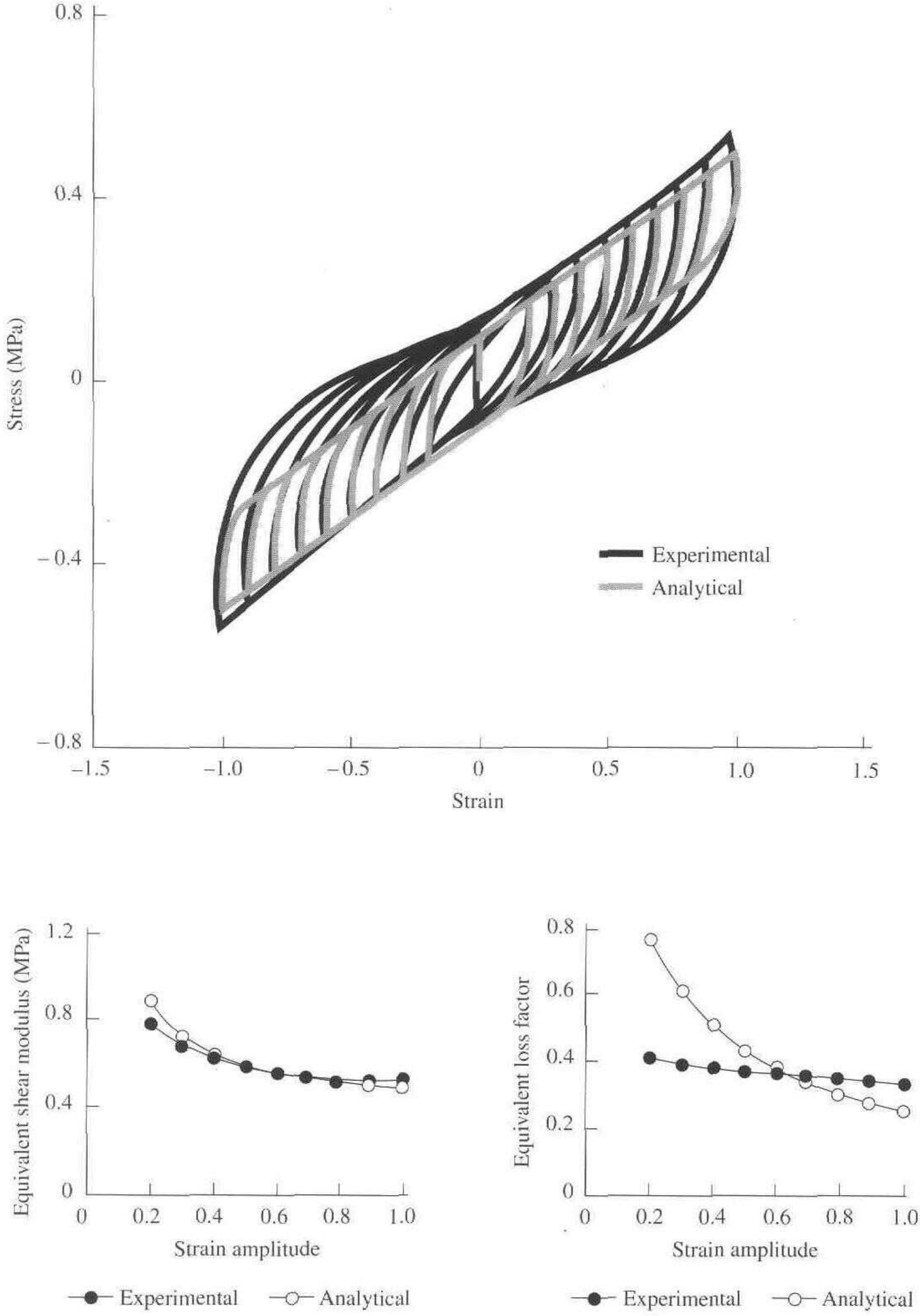

Figure 4. Comparison of results from experiments and LAM.

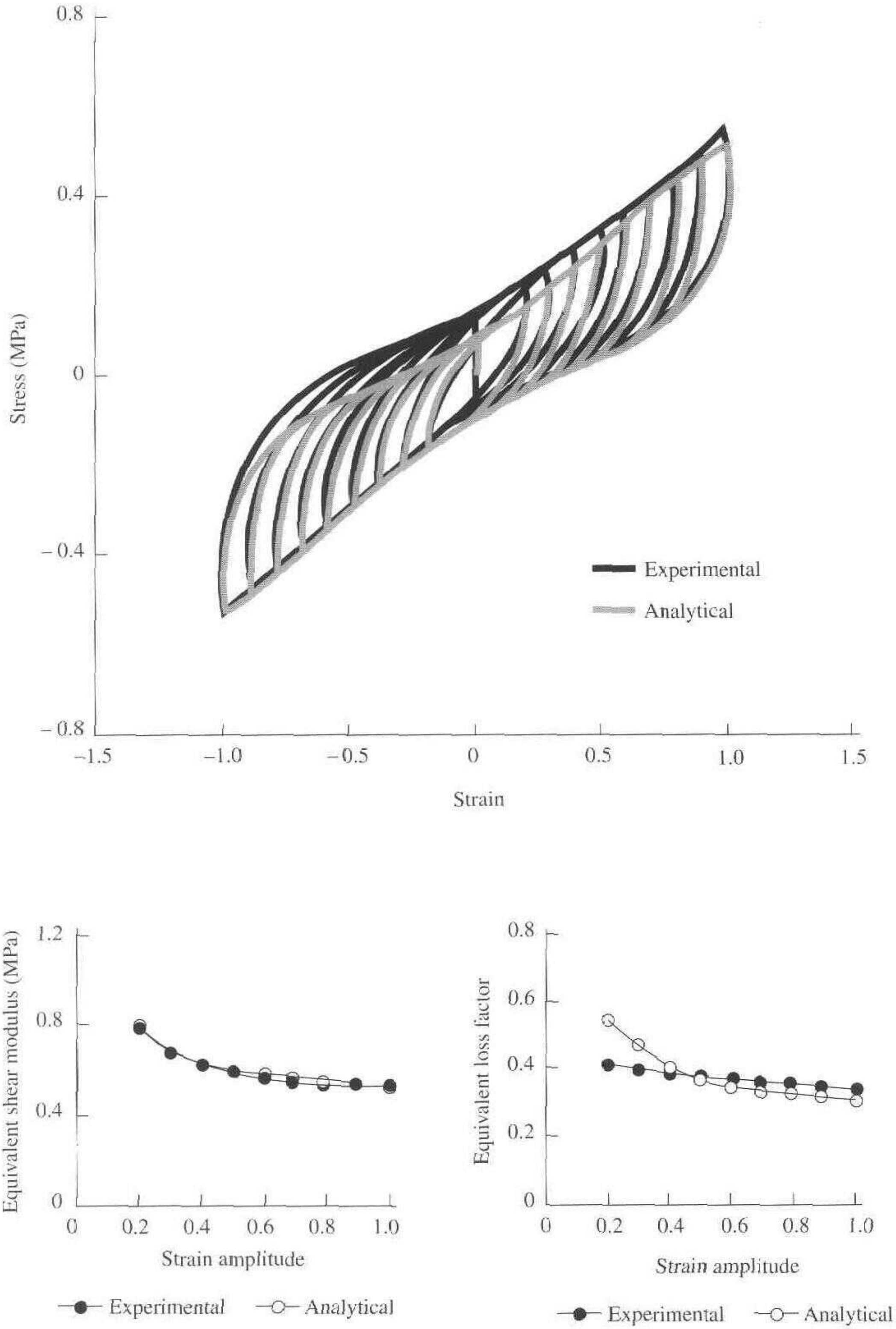

Figure 5. Comparison of results from experiments and FPAM.

a strain reversal is too small compared to the experimental results. The FAPM can be improved to overcome this observed shortcoming by modifying the e/e_0 term, which varies from 1 at the point of strain reversal to an infinitesimal value as the stress-strain path approaches the asymptote.

Fourth Order Polynomial Asymptote and Power Function Model (FPAPM)

To overcome the observed shortcoming of the FAPM, *Equation 8* is rewritten with the e/e_0 term raised to the power N as follows:

$$\frac{d\tau}{d\gamma} = \frac{d\bar{\tau}(\gamma)}{d\gamma}\left\{1 + k\left[\frac{e}{e_0}\right]^{N}\right\} \qquad \text{... 10}$$

where, $d\bar{\tau}(\gamma)/d\gamma$, $\tau_1(\gamma)$, $\tau_2(\gamma)$, e, e_0, γ_0, τ_0, k, A_1, A_2, A_3, A_4, and A_5 are as defined for *Equation 8*.

The solution to *Equation 10* provides the following closed-form expression for $\tau(\gamma)$:

$$\tau(\gamma) = \bar{\tau}(\gamma) - e_0\left[1 - \frac{\overline{W}(\gamma)\,k(\gamma_0 - \gamma)(N-1)}{e_0}\right]^{\frac{1}{1-N}} \qquad \text{... 11}$$

where, $\bar{\tau}(\gamma) = \tau_1(\gamma)$ and $\overline{W}(\gamma) = W_1(\gamma)$ for loading;

$\bar{\tau}(\gamma) = \tau_2(\gamma)$ and $\overline{W}(\gamma) = W_2(\gamma)$ for unloading;

$W_1(\gamma)$ and $W_2(\gamma)$ are as defined for *Equation 9*; and

$N \neq 1$.

Similar to *Equation 7* and *Equation 9*, the right side of *Equation 11* has two terms. The first term is the target asymptote and the second term decays as the magnitude of $(\gamma_0 - \gamma)$ increases. *Equation 11* has seven parameters, A_1, A_2, A_3, A_4, A_5, k, and N, to be determined from experimental data. A value of 2 was selected for N before the remaining parameters were determined by non-linear regression. *Equation 11* rewritten with N = 2 is as follows:

$$\tau(\gamma) = \bar{\tau}(\gamma) - e_0\left[1 - \frac{\overline{W}(\gamma)\,k\,(\gamma_0 - \gamma)}{e_0}\right]^{-1} \qquad \text{... 12}$$

Values of the parameters, A_1, A_2, A_3, A_4, A_5, and k, determined from non-linear regression are given in *Table 2*. Analytical hysteresis loops, generated using *Equation 12* with these parameter values, are compared with experimental hysteresis loops in *Figure 6*. Good agreement between the analytical and experimental results is observed for hysteresis loops with a strain amplitude between 20% and 100%.

PARAMETER ESTIMATION

The values of the parameters were estimated using non-linear regression in the stress-strain plane. The parameter values are those that satisfy the following least-squares condition:

$$\text{Minimise} \quad \sum_i \sum_j \left[\tau_{exp}(i,j) - \tau_{mod}(i,j)\right]^2 \qquad \text{... 13}$$

where, i = index for data set at a specific strain amplitude (*e.g.*, i = 1, strain amplitude = 20%);

j = index for a stress-strain point within the data set at a specific strain amplitude;

$\tau_{exp}(i,j)$ = stress data point from experiments;

$\tau_{mod}(i,j)$ = stress calculated from either *Equation 7*, *Equation 9*, or *Equation 12* using $\gamma_{exp}(i,j)$; and

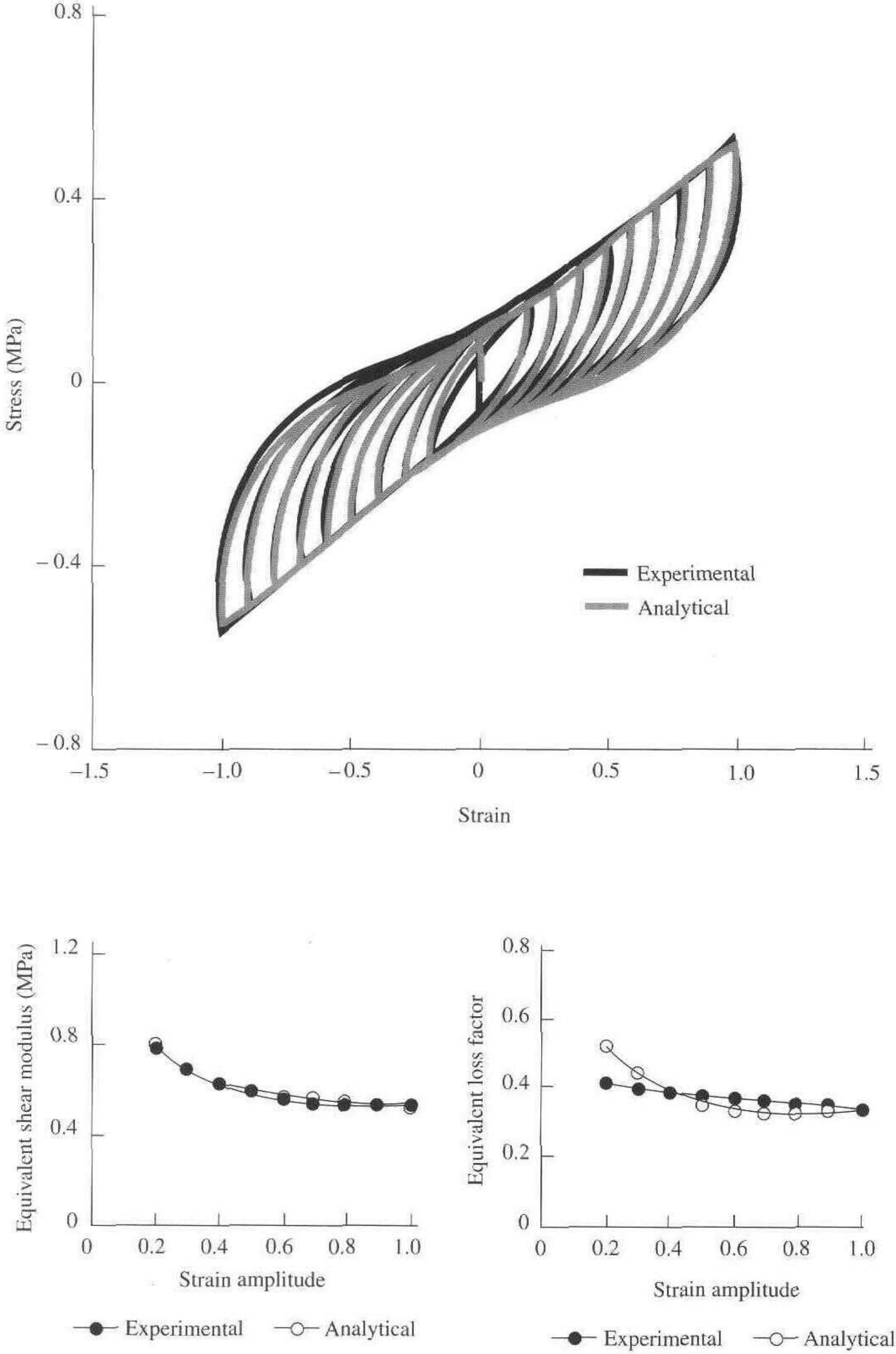

Figure 6. Comparison of results from experiments and FPAPM.

$\gamma_{exp}(i,j)$ = stain data point from experiments corresponding to $\tau_{exp}(i,j)$

Since the experimental hysteresis loops are slightly unsymmetric about the origin, data from both the loading (positive increment of strain) direction and the unloading (negative increment of strain) direction were used in the non-linear regression

Figure 7(a) shows a typical hysteresis loop and *Figure 7(b)* shows details of this hysteresis loop near the point of maximum strain Between the point of maximum stress and the point of maximum strain, the experimental hysteresis loop in *Figure 7(b)* has a negative slope, which is assumed to be caused by a (small) rate dependent behaviour of the UHDNR material The rate-independent models presented previously will not capture this behaviour Thus this region of negative stiffness was removed from the experimental data [*Figure 7(c)*] before the data was used in the non-linear regression, and a better overall fit of the experimental data was obtained

The hysteresis models presented earlier have separate (but similar) functions for the loading and unloading directions Thus the experimental data was divided into loading and unloading segments The solid circle at the maximum stress and strain shown in *Figure 7(c)*, defines the end of a loading segment and the start of an unloading segment A similar point at the minimum stress and strain defines the end of an unloading segment and the starting point of a loading segment As shown in *Figure 7(c)* the experimental hysteresis loops do not actually include these points, but the rate-independent models presented previously will pass through these peak points The Marquardt algorithm[6] was used to minimise the error expression in *Equation 13* The parameter values for the models presented earlier are given in *Table 3*

Sequential Asymptote Model for Random Loading

The analytical hysteresis loops shown in *Figure 6*, generated using FPAPM (*Equation 12*), are for the case of sinusoidal loading with increasing strain amplitude For random loading, direct application of *Equation 12* may not give satisfactory results because a small strain reversal followed by a second strain reversal (so that the strain continues in the original direction of loading) may cause the new stress-strain path to overshoot significantly the stress strain path that would be followed without the strain reversals *Figure 8* illustrates this problem Two imposed strain histories are shown in *Figure 8(a)* The first is a sinusoidal function with decreasing amplitude The second is a decreasing-amplitude sinusoidal function with very small strain reversals, ±0 02 placed within the function Since FPAPM (*Equation 12*) is a rate independent hysteresis model, this change to the loading history should be inconsequential *Figure 8(b)* shows the hysteresis loops generated using FPAPM A comparison of the two sets of loops shows that a small strain reversal causes the stress-strain path to overshoot the correct path immediately after the reversal

To overcome this problem, a sequential asymptote model (SAM) is used with FPAPM The sequential asymptote model uses an algorithm that allows a sequence of asymptotes to be maintained to prevent the stress-strain path from overshooting a previous stress-strain path as a result of strain reversals under random loading *Figure 9* illustrates the sequential asymptote model Unlike FPAPM (*Equation 12*), which considers only a single asymptote for each loading direction SAM considers a sequence of asymptotes, where the first asymptote is the original asymptote [either $\tau_1(\gamma)$ or $\tau_2(\gamma)$] and each subsequent asymptote is a previously defined stress-strain path

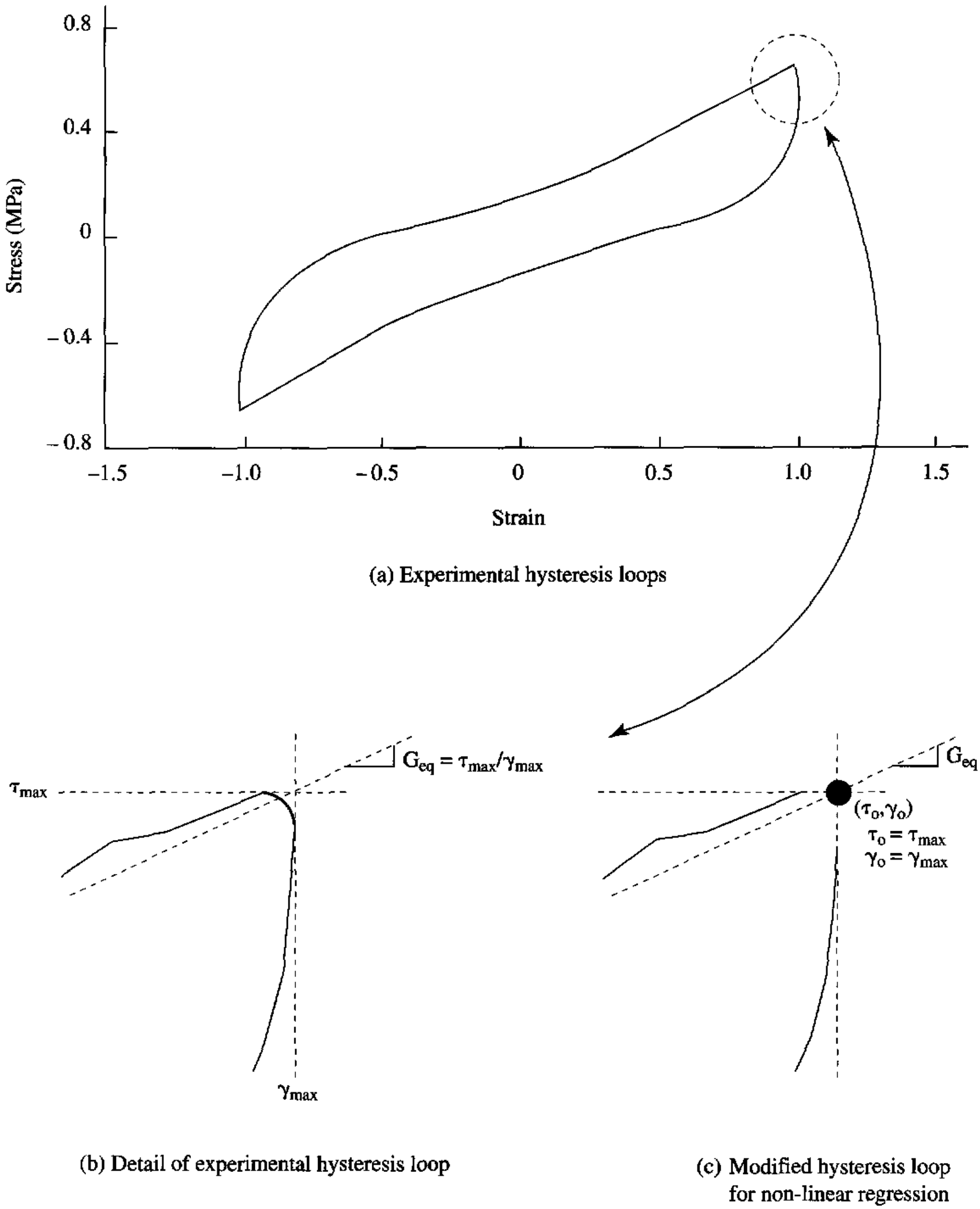

Figure 7. Modified experimental data for non-linear regression.

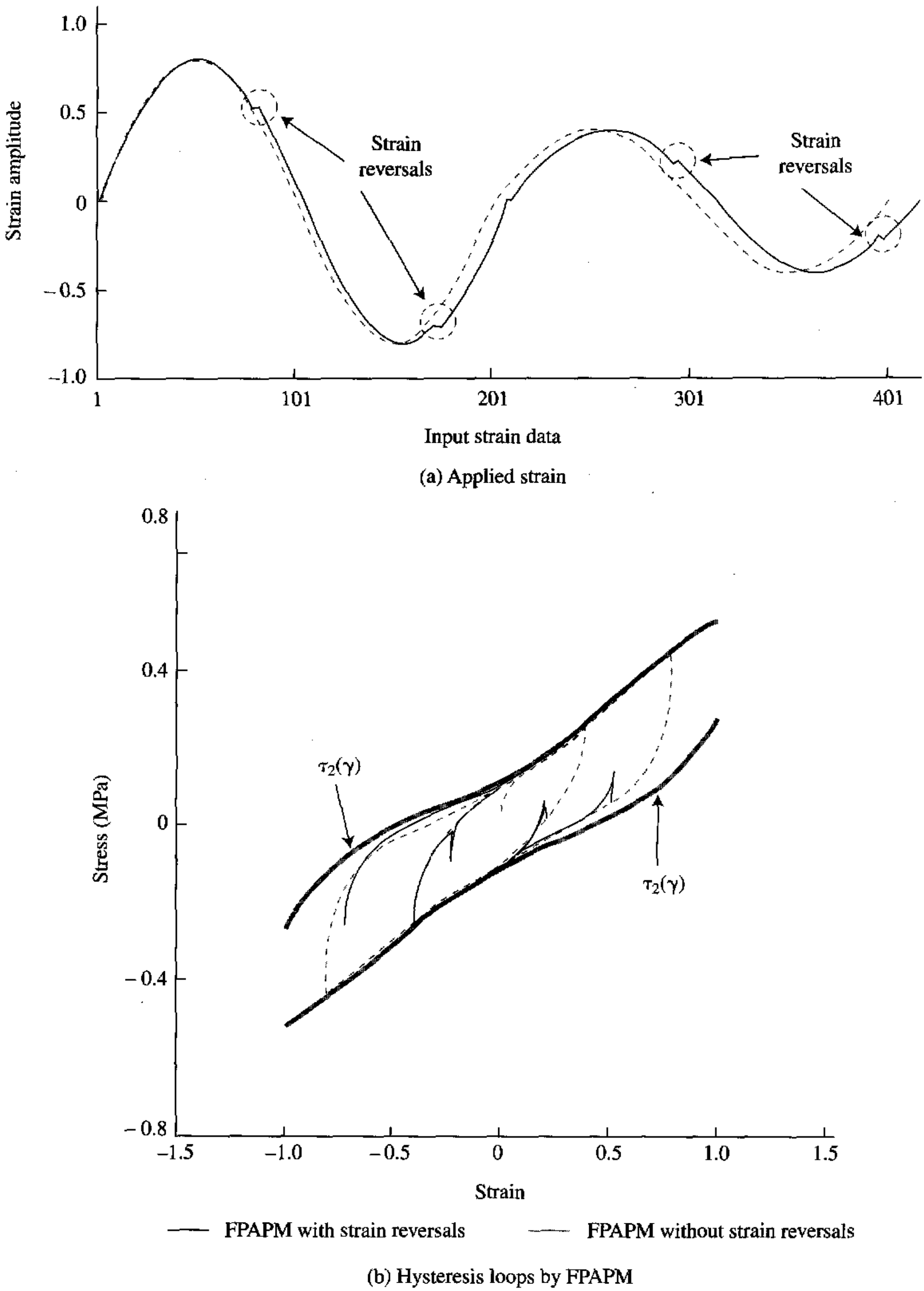

Figure 8. Hysteresis loops under random loading.

[*Figure 9(a)*]. As shown in *Figure 9(b)*, a new asymptote is defined at a strain reversal if the absolute value of the strain at the reversal is less than the absolute value of the strain at the strain reversal associated with the most recently defined stress-strain path in the same loading direction.

The following discussion explains the hysteresis model that uses FPAPM with SAM. The combined model uses FPAPM to define the initial asymptotes and the basic form of the asymptotic functions, while SAM provides the basis for defining subsequent asymptotes. The FPAPM equation, *Equation 12*, is rewritten using subscripts to keep track of the most recently defined asymptote in each direction of loading, as follows. For the loading direction [*Figure 9(b)*],

$$\tau_{(1,1)}(\gamma) = \tau_1(\gamma) - e_{0(1,1)}\left[1 - \frac{W_{(1,1)}(\gamma)\,k_{(1,1)}[\gamma_{0(1,1)}-\gamma]}{e_{0(1,1)}}\right]^{-1} \quad \ldots 14-1$$

where, $\tau_1(\gamma) = A_1\gamma^4+A_2\gamma^3+A_3\gamma^2+A_4\gamma+A_5$;

$e_{0(1,1)} = \tau_1(\gamma_{0(1,1)}) - \tau_{0(1,1)}$;

$\tau_1(\gamma_{0(1,1)}) = \tau_1(\gamma)$ evaluated at $\gamma = \gamma_{0(1,1)}$;

$W_{(1,1)}(\gamma) = A_1[\gamma^3+\gamma^2\gamma_{0(1,1)}+\gamma\gamma_{0(1,1)}^2+\gamma_{0(1,1)}^3] + A_2[\gamma^2+\gamma\gamma_{0(1,1)} + \gamma_{0(1,1)}^2] + A_3[\gamma+\gamma_{0(1,1)}] + A_4$;
$k_{(1,1)} = k$; and

$\gamma_{0(1,1)}$ and $\tau_{0(1,1)}$ are the strain and stress at the 1st strain reversal for the loading direction.

For the unloading direction,

$$\tau_{(2,1)}(\gamma) = \tau_2(\gamma) - e_{0(2,1)}\left[1 - \frac{W_{(2,1)}(\gamma)\,k_{(2,1)}[\gamma_{0(2,1)}-\gamma]}{e_{0(2,1)}}\right]^{-1} \quad \ldots 14-2$$

where, $\tau_2(\gamma) = -A_1\gamma^4+A_2\gamma^3-A_3\gamma^2+A_4\gamma-A_5$;

$e_{0(2,1)} = \tau_2(\gamma_{0(2,1)}) - \tau_{0(2,1)}$;

$\tau_2(\gamma_{0(2,1)}) = \tau_2(\gamma)$ evaluated at $\gamma = \gamma_{0(2,1)}$;

$W_{(2,1)}(\gamma) = -A_1[\gamma^3+\gamma^2\gamma_{0(2,1)}+\gamma\gamma_{0(2,1)}^2+\gamma_{0(2,1)}^3] + A_2[\gamma^2+\gamma\gamma_{0(2,1)} + \gamma_{0(2,1)}^2] - A_3[\gamma+\gamma_{0(2,1)}] + A_4$
$k_{(2,1)} = k$; and

$\gamma_{0(2,1)}$ and $\tau_{0(2,1)}$ are the strain and stress at the 1st strain reversal for the unloading direction.

In the above expressions, the first subscript in parentheses identifies the loading direction and the second subscript identifies the stress-strain path for each direction. $\gamma_{0(1,1)}$ and $\gamma_{0(2,1)}$ are the strains at the 1st strain reversal in each direction. $\tau_{0(1,1)}$ and $\tau_{0(2,1)}$ are the stresses at the 1st strain reversal in each direction.

Stress-strain paths within a complex loading history are now considered. The 1st strain reversal in each direction defines the 1st stress-strain path in each direction. *Figure 9(b)* shows a strain reversal at $\gamma_{0(1,2)}$. Prior to this 2nd strain reversal, the 1st strain reversal occurred at $\gamma_{0(1,1)}$, so the stress-strain path $\tau_{(1,2)}(\gamma)$ after the 2nd strain reversal at $\gamma_{0(1,2)}$ is asymptotic to the 1st stress-strain path, $\tau_{(1,1)}(\gamma)$, which is asymptotic to the original asymptote, $\tau_1(\gamma)$.

The stress-strain path in *Figure 9(b)* is as follows:

$$\tau_{(1,2)}(\gamma) = \tau_1(\gamma) - e_{0(1,1)}\left[1 - \frac{W_{(1,1)}(\gamma)\,k_{(1,1)}[\gamma_{0(1,1)}-\gamma]}{e_{0(1,1)}}\right]^{-1} - e_{0(1,2)}\left[1 - \frac{W_{(1,2)}(\gamma)\,k_{(1,2)}[\gamma_{0(1,2)}-\gamma]}{e_{0(1,2)}}\right]^{-1} \quad \ldots 15$$

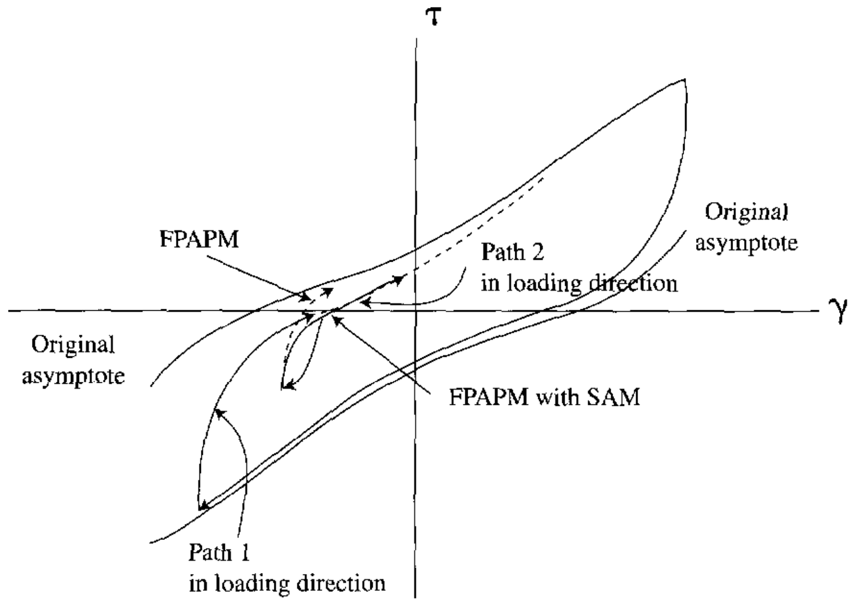

(a) Comparison of FPAPM and FPAPM with SAM

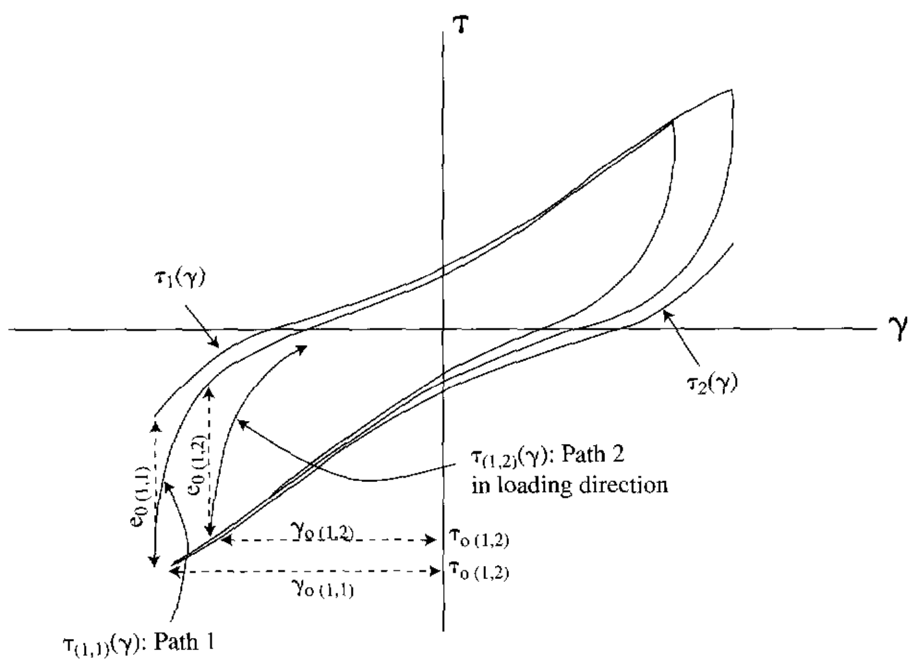

(b) Notation for SAM

Figure 9. Schematic of the sequential asymptote model (SAM).

where, $\tau_1(\gamma)$, $e_{0(1,1)}$, $W_{(1,1)}(\gamma)$, $k_{(1,1)}$, and $\gamma_{0(1,1)}$ are as defined for *Equation 14–1*;

$W_{(1,2)}(\gamma) = A_1[\gamma^3+\gamma^2\gamma_{0(1,2)}+\gamma\gamma_{0(1,2)}^2+\gamma_{0(1,2)}^3] + A_2[\gamma^2+\gamma\gamma_{0(1,2)}+\gamma_0^2] + A_3[\gamma^2+\gamma_{0(1,2)}] + A_4$;

$k_{(1,2)}$ and $e_{0(1,2)}$ are determined as described later; and

$\gamma_{0(1,2)}$ is the strain at the 2nd strain reversal for the loading direction.

Considering the possibility of a sequence of strain reversals, a general expression for a stress-strain path in the loading direction, $\tau_{(1,i)}(\gamma)$, is obtained by generalising *Equation 15* as follows:

$$\tau_{(1,i)}(\gamma) = \tau_1(\gamma) - \sum_{j=1} e_{0(1,j)} \left[1 - \frac{W_{(1,j)}(\gamma)\,k_{(1,j)}[\gamma_{0(1,j)} - \gamma]}{e_{0(1,j)}}\right]^{-1} \quad \text{... 16–1}$$

where, $W_{(1,j)}(\gamma) = A_1[\gamma^3+\gamma^2\gamma_{0(1,j)}+\gamma\gamma_{0(1,j)}^2+\gamma_{0(1,j)}^3] + A_2[\gamma^2+\gamma\gamma_{0(1,j)}+\gamma_0^2] + A_3[\gamma+\gamma_{0(1,j)}] + A_4$;

$k_{(1,j)}$ and $e_{0(1,j)}$ are determined as described later; and

$\gamma_{0(1,j)}$ is the strain at the jth strain reversal for the loading direction.

Similarly, the general expression for a stress-strain path in the unloading direction, $\tau_{(2,i)}(\gamma)$, is as follows:

$$\tau_{(2,i)}(\gamma) = \tau_2(\gamma) - \sum_{j=1} e_{0(2,j)} \left[1 - \frac{W_{(2,j)}(\gamma)\,k_{(2,j)}[\gamma_{0(2,j)} - \gamma]}{e_{0(2,j)}}\right]^{-1} \quad \text{... 16–2}$$

where, $W_{(2,j)}(\gamma) = -A_1[\gamma^3+\gamma^2\gamma_{0(2,j)}+\gamma\gamma_{0(2,j)}^2+\gamma_{0(2,j)}^3] + A_2[\gamma^2+\gamma\gamma_{0(2,j)}+\gamma_0^2] - A_3[\gamma+\gamma_{0(2,j)}] + A_4$;

$k_{(2,j)}$ and $e_{0(2,j)}$ are determined as described later; and

$\gamma_{0(2,j)}$ is the strain at the jth strain reversal for the unloading direction.

Equation 16 – 1 and *Equation 16 – 2* show that the current stress-strain path i requires information (*e.g.*, $W_{(1,j)}$, $k_{(1,j)}$, $e_{0(1,j)}$, and $\gamma_{0(1,j)}$) which is related to each previous stress-strain path j, j = 1...i–1, as well as information (*e.g.* $W_{(1,i)}$, $k_{(1,i)}$, $e_{0(1,i)}$, and $\gamma_{0(1,i)}$) for the current stress-strain path i. $W_{(1,i)}$ and $\gamma_{0(1,i)}$ have already been described. $W_{(1,i)}$ depends on only the strain at strain reversal i, $\gamma_{0(1,i)}$. However, $e_{0(1,i)}$ and $k_{(1,i)}$ must be determined from the previous loading history when stress-strain path i is established (at $\gamma = \gamma_{0(1,i)}$).

$e_{0(1,i)}$ is the stress deviation between the asymptote for stress-strain path i and the stress at the strain reversal that defines the beginning of stress-strain path i, $\tau_{0(1,i)}$. Since the asymptote for stress-strain path i is, in general, the most recent stress-strain path (path i–1) in the same loading direction, $e_{0(1,i)}$ (and similarly $e_{0(2,i)}$ for *Equation 16 – 2*) is easily calculated. For example, for the 2nd stress-strain path in the loading direction (*Equation 15*),

$$e_{0(1,2)} = \tau_1(\gamma_{0(1,2)}) - e_{0(1,1)} \left[1 - \frac{W_{(1,1)2}\,k_{(1,1)}\Delta\gamma_{(1,1)2}}{e_{0(1,1)}}\right]^{-1} - \tau_{0(1,2)} \quad \text{... 17}$$

where, $\tau_1(\gamma_{0(1,2)}) = \tau_1(\gamma)$ evaluated at $\gamma = \gamma_{0(1,2)}$;

$W_{(1,1)2} = W_{(1,1)}(\gamma)$ evaluated at $\gamma = \gamma_{0(1,2)}$;

$A_1[\gamma_{0(1,2)}^3+\gamma_{0(1,2)}^2\gamma_{0(1,1)}+\gamma_{0(1,2)}\gamma_{0(1,1)}^2+\gamma_{0(1,1)}^3]+A_2[\gamma_{0(1,2)}^2+\gamma_{0(1,2)}\gamma_{0(1,1)}+\gamma_{0(1,1)}^2]+A_3[\gamma_{0(1,2)}+\gamma_{0(1,1)}]+A_4$;

$\Delta\gamma_{(1,1),2} = \gamma_{0(1,1)} - \gamma_{0(1,2)}$; and

$\tau_{0(1,2)}$ is the stress at the 2nd strain reversal for the loading direction.

In *Equation 17*, the first two terms equal the stress on the asymptote for the 2nd stress-strain path in the loading direction at the strain reversal (at $\gamma = \gamma_{0(1,2)}$) that defines the beginning of the 2nd stress-strain path. These are obtained by substituting $\gamma_{0(1,2)}$ into the function for stress on the 1st stress-strain path in the loading direction *Equation 14–1*. The general expression for $e_{0(1,i)}$ is:

$$e_{0(1,i)} = \tau_1(\gamma_{0(1,i)}) - \sum_{j=1}^{i-1} \left\{ e_{0(1,j)} \left[1 - \frac{W_{(1,j)i}\, k_{(1,j)}\, \Delta\gamma_{0(1,j)i}}{e_{0(1,j)}} \right]^{-1} \right\} - \tau_{0(1,i)} \qquad \ldots\ 18\text{–}1$$

where, $\tau_1(\gamma_{0(1,i)}) = \tau_1(\gamma)$ evaluated at $\gamma = \gamma_{0(1,i)}$;

$W_{(1,j),i} = W_{(1,j)}(\gamma)$ evaluated at $\gamma = \gamma_{0(1,i)}$

$=A_1[\gamma_{0(1,i)}^3+\gamma_{0(1,i)}^2\gamma_{0(1,j)}+\gamma_{0(1,i)}\gamma_{0(1,j)}^2+\gamma_{0(1,j)}^3]+A_2[\gamma_{0(1,i)}^2+\gamma_{0(1,i)}\gamma_{0(1,j)}+\gamma_{0(1,j)}^2]+A_3[\gamma_{0(1,i)}+\gamma_{0(1,j)}]+A_4$;

$\Delta\gamma_{(1,j),i} = \gamma_{0(1,j)} - \gamma_{0(1,i)}$; and

$\tau_{0(1,i)}$ is the stress at the ith strain reversal for the loading direction.

Equation 18–1 is established by generalising *Equation 17*, considering the possibility of a sequence of strain reversals. Note that for the 1st stress-strain path (*i.e.* for i = 1), the summation in *Equation 18–1* equals zero (*i.e.* for j = 1…0, the summation is zero), and, therefore, *Equation 18–1* degenerates to the definition of $e_{0(1,1)}$ given with *Equation 14–1*. A similar general expression for $e_{0(2,i)}$ is

$$e_{0(2,i)} = \tau_1(\gamma_{0(2,i)}) - \sum_{j=1}^{i-1} \left\{ e_{0(2,j)} \left[1 - \frac{W_{(2,j)i}\, k_{(2,j)}\, \Delta\gamma_{0(2,j)i}}{e_{0(2,j)}} \right]^{-1} \right\} - \tau_{0(2,i)} \qquad \ldots\ 18\text{–}2$$

where, $W_{(2,j),i} = W_{(2,j)}(\gamma)$ evaluated at $\gamma = \gamma_{0(2,i)}$

$=A_1[\gamma_{0(2,i)}^3+\gamma_{0(2,i)}^2\gamma_{0(2,j)}+\gamma_{0(2,i)}\gamma_{0(2,j)}^2+\gamma_{0(2,j)}^3]+A_2[\gamma_{0(2,i)}^2+\gamma_{0(2,i)}\gamma_{0(2,j)}+\gamma_{0(2,j)}^2]-A_3[\gamma_{0(2,i)}+\gamma_{0(2,j)}]+A_4$;

$\Delta\gamma_{(2,j),i} = \gamma_{0(2,j)} - \gamma_{0(2,i)}$; and

$\tau_{0(2,i)}$ is the stress at the ith strain reversal for the unloading direction.

$k_{(1,i)}$ and $k_{(2,i)}$ are similar to k, which, as discussed earlier, is determined from a non-linear regression. $k_{(1,i)}$ and $k_{(2,i)}$ are derived assuming that the instantaneous stiffness at a point of strain reversal equals the slope of the original asymptote [$\tau_1(\gamma)$ or $\tau_2(\gamma)$] at the strain corresponding to the strain reversal ($\gamma_{0(1,i)}$ or $\gamma_{0(2,i)}$) multiplied by $(1 + k)$. As a result of this assumption, the instantaneous stiffness at a strain reversal depends only on the strain at the reversal, not on the loading history, and this instantaneous stiffness at strain reversal is consistent with that of FPAM (*Equation 8*) and FPAPM (*Equation 10*). For example, to derive $k_{(1,2)}$ *Equation 15* is differentiated:

$$\frac{d\tau_{(1,2)}(\gamma)}{d\gamma} = \frac{d\tau_1(\gamma)}{d\gamma} + k_{(1,1)}$$

$$\left\{-\frac{dW_{(1,1)}(\gamma)}{d\gamma}[\gamma_{0(1,1)} - \gamma] + W_{(1,1)}(\gamma)\right\}$$

$$\left\{1 - \frac{W_{(1,1)}(\gamma)k_{(1,1)}[\gamma_{0(1,1)} - \gamma]}{e_{0(1,1)}}\right\}^{-2}$$

$$+ k_{(1,2)}\left\{-\frac{dW_{(1,2)}(\gamma)}{d\gamma}[\gamma_{0(1,2)} - \gamma] + W_{(1,2)}(\gamma)\right\}$$

$$\left\{1 - \frac{W_{(1,2)}(\gamma)k_{(1,2)}[\gamma_{0(1,2)} - \gamma]}{e_{0(1,2)}}\right\}^{-2} \quad \ldots 19$$

After substituting $\gamma = \gamma_{0(1,2)}$ into *Equation 19* and equating the right side of *Equation 19* to $\frac{d\tau_1(\gamma)}{d\gamma}(1 + k)$ evaluated at $\gamma = \gamma_{0(1,2)}$, $k_{(1,2)}$ is expressed as:

$$k_{(1,2)} = k_{(1,1)}$$

$$\left\{1 - \frac{[-DW_{(1,1)2}\Delta\gamma_{(1,1)2} + W_{(1,2)2}]\left[1 - \frac{W_{(1,1),2}k_{(1,1)}\Delta\gamma_{(1,1)2}}{e_{0(1,1)}}\right]^{-2}}{W_{(1,2)2}}\right\} \quad \ldots 20$$

where, $DW_{(1,1),2} = \frac{dW_{(1,1)}(\gamma)}{d\gamma}$ evaluated at $\gamma = \gamma_{0(1,2)}$

$= A_1[3\gamma_0{}^2{}_{(1,2)} + 2\gamma_{0(1,2)}\gamma_{0(1,1)} + \gamma_0{}^2{}_{(1,1)}] + A_2[2\gamma_{0(1,2)} + \gamma_{0(1,1)}] + A_3$;

$\Delta\gamma_{(1,1),2}$ and $W_{(1,1),2}$ are defined with *Equation 17*;

$W_{(1,2),2} = W_{(1,2)}(\gamma)$ evaluated at $\gamma = \gamma_{0(1,2)}$

$= 4A_1\gamma_0{}^3{}_{(1,2)} + 3A_3\gamma_0{}^2{}_{(1,2)} + 2A_3\gamma_{0(1,2)} + A_4$; and

$k_{(1,1)} = k$.

Considering the possibility of a sequence of strain reversals, the general expression for $k_{(1,i)}$ is:

$$k_{(1,i)} = k_{(1,1)} - \sum_{j=1}^{i-1}$$

$$\left\{k_{(1,j)}\frac{[-DW_{(1,j),i}\Delta\gamma_{(1,j),i} + W_{(1,j),i}]\left[1 - \frac{W_{(1,j),i}k_{(1,j)}\Delta\gamma_{(1,j),i}}{e_{0(1,j)}}\right]^{-2}}{W_{(1,i),i}}\right\} \quad \ldots 21\text{–}1$$

where, $DW_{(1,j),i} = \frac{dW_{(1,j)}(\gamma)}{d\gamma}$ evaluated at $\gamma = \gamma_{0(1,i)}$

$= A_1[3\gamma_0{}^2{}_{(1,i)} + 2\gamma_{0(1,i)}\gamma_{0(1,j)} + \gamma_0{}^2{}_{(1,j)}] + A_2[2\gamma_{0(1,i)} + \gamma_{0(1,j)}] + A_3$;

$\Delta\gamma_{(1,j),i}$ and $W_{(1,j),i}$ are defined with *Equation 18–1*; and

$W_{(1,i),i} = W_{(1,i)}(\gamma)$ evaluated at $\gamma = \gamma_{0(1,i)}$

$= 4A_1\gamma_0{}^3{}_{(1,i)} + 3A_2\gamma_0{}^2{}_{(1,i)} + 2A_3\gamma_{0(1,i)} + A_4$.

Similarly, the general expression for $k_{(2,i)}$ is:

$$k_{(2,i)} = k_{(2,1)} - \sum_{j=1}^{i-1}$$

$$\left\{k_{(2,j)}\frac{[-DW_{(2,j),i}\Delta\gamma_{(2,j),i} + W_{(2,j),i}]\left[1 - \frac{W_{(2,j),i}k_{(2,j)}\Delta\gamma_{(2,j),i}}{e_{0(2,j)}}\right]^{-2}}{W_{(2,i),i}}\right\} \quad \ldots 21\text{–}2$$

where, $DW_{(2,j),i} = \frac{dW_{(2,j)}(\gamma)}{d\gamma}$ evaluated at $\gamma = \gamma_{0(2,i)}$

$= -A_1[3\gamma_0{}^2{}_{(2,i)} + 2\gamma_{0(2,i)}\gamma_{0(2,j)} + \gamma_0{}^2{}_{(2,j)}] + A_2[2\gamma_{0(2,i)} + \gamma_{0(2,j)}] - A_3$;

$\Delta\gamma_{(2,j),i}$ and $W_{(2,j),i}$ are defined with *Equation 18–2*:

$$W_{(2,i),i} = W_{(2,i)}(\gamma) \text{ evaluated at } \gamma = \gamma_{0(2,i)}$$

$$= 4A_1\gamma_0{}^3_{(2,i)} + 3A_2\gamma_0{}^2_{(2,i)} + 2A_3\gamma_{0(2,i)} + A_4;$$

and $k_{(2,i)} = k$.

FPAPM with SAM, as defined by *Equation 16–1* and *16–2*, *Equation 18–1* and *18–2*, and *Euation 21–1* and *21–2*, maintains three sets of quantities, $\gamma_{0(LST,j)}$, $e_{0(LST,j)}$, and $k_{0(LST,j)}$, which define individual stress-strain paths j = 1,2,3…i, where i is the current stress-strain path. LST is 1 for the loading direction or 2 for the unloading direction. The quantities for the stress-strain paths are ordered so that the absolute value of $\gamma_{0(LST,j)}$ is less than the absolute value of $\gamma_{0(LST,j-1)}$, and therefore $\gamma_{0(LST,i)}$ has the smallest absolute value. Whenever a strain reversal occurs, the strain at the strain reversal is compared with the strains at the previous reversals for that direction, $\gamma_{0(LST,j)}$.

If the absolute value of the strain at the new strain reversal is less than the absolute value of $\gamma_{0(LST,i)}$, then a new stress-strain path is established as follows: i is incremented by 1; the strain at the new reversal becomes the new $\gamma_{0(LST,i)}$; and $e_{0(LST,i)}$ and $k_{0(LST,i)}$ are calculated and the new stress-strain path i is established.

If the absolute value of the strain at the new strain reversal is greater than or equal to the absolute value of one value in $\gamma_{0(LST,j)}$, say $\gamma_{0(LST,m)}$, then a new stress-strain path is established as follows: all of the quantities $\gamma_{0(LST,j)}$, $e_{0(LST,j)}$, and $k_{0(LST,j)}$ for j = m…i are discarded; i is set equal to m; the strain at the new reversal becomes the new $\gamma_{0(LST,i)}$; and $e_{0(LST,i)}$ and $k_{0(LST,i)}$ are calculated and the new stress-strain path i is established.

Compared to FPAPM alone (*Equation 12*) which is based on the local loading history, FPAPM with SAM more accurately accounts for the loading history under random loading. *Figure 10* shows the hysteresis loops generated using FPAPM with SAM. Good agreement is observed between data generated with FPAPM when small strain reversals are not included in the history, and FPAPM with SAM when small strain reversals are included.

CONCLUSIONS

A series of experiments on UHDNR structural dampers were summarised. Compared to HDR used in base isolation system, the loss factor for UHDNR structural dampers is quite high, between 0.35 and 0.40.

Rate-independent models for the hysteresis behaviour of UHDNR structural dampers under dynamic loading have been presented. The fourth order polynomial with power function model (FPAPM) was quite accurate when compared to the experimental data for strain amplitudes less than 100%. However, the parameters determined from fitting the FPAPM model to the experimental data should be verified using other UHDNR experimental data sets.

The fourth order polynomial with power function model (FPAPM) combined with SAM more accurately accounts for the loading history under random loading than FPAPM alone. In particular, when the loading history includes a series of small strain reversals, FPAPM combined with SAM avoids the problem of overshooting the stress-strain path that would be followed without the strain reversals.

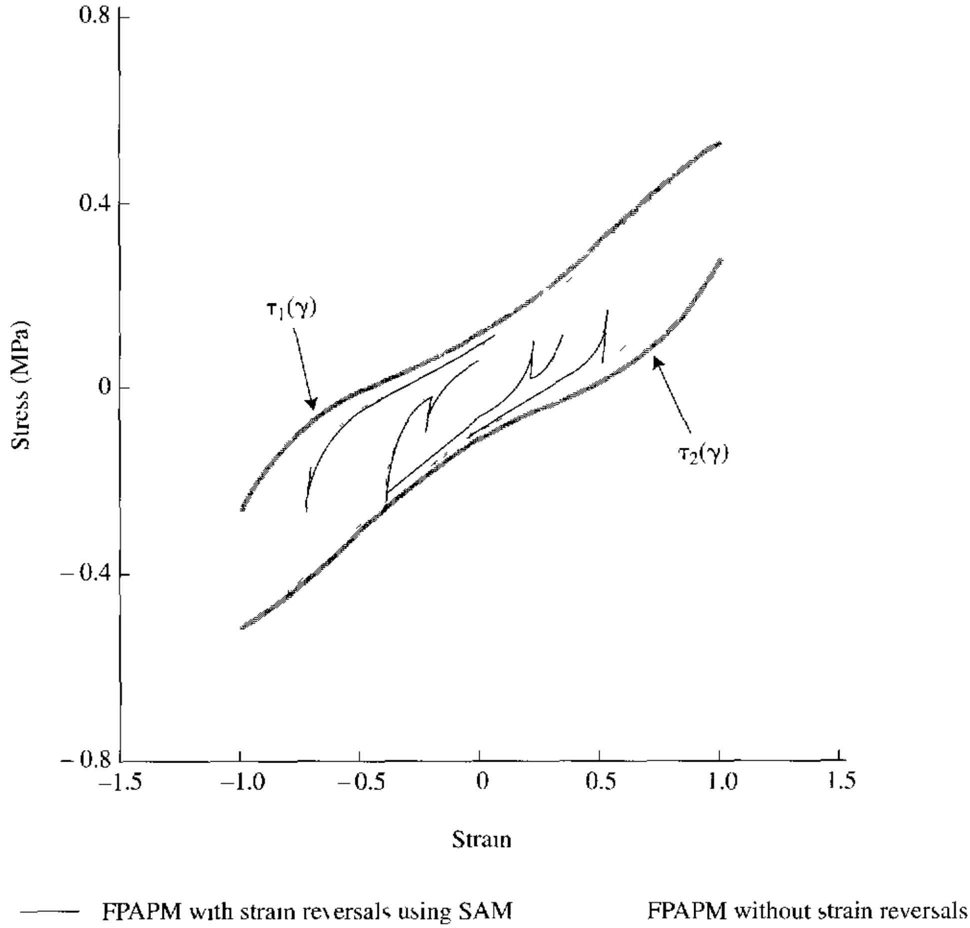

Figure 10. Hysteresis loops using FPAPM with SAM under random loading.

ACKNOWLEDGEMENT

The authors wish to thank the Director General of the Malaysian Rubber Board for permission to publish this paper and the Malaysian Rubber Board for funding the research which was conducted at the Center for Advanced Technology for Large Structural Systems (ATLSS) at Lehigh University. We also like to thank Dr K. Fuller of the Tun Abdul Razak Laboratory, Malaysian Rubber Board, United Kingdom, for useful discussions on the high damping natural rubber compounds. The assistance of the ATLSS technical staff, in particular Dr. E. Kaufmann, E. Tomlinson, J. Hoffner, J. Pinter, and a graduate student, B. Metrovich, with the experiments is also acknowledged.

Date of receipt: July 2001
Date of acceptance: October 2001

REFERENCES

1 AHMADI, H R, MUHR, A H (1996) Modeling the Dynamic Properties of Filled Rubber *International Rubber Conference, Manchester, UK*

2 CLOUGH R W AND PENZIEN, J (1975) *Dynamics of Structures*, 1st Edition New York McGraw-Hill Inc

3 HWANG, J S AND WANG, J C (1998) Seismic Response Prediction of HDR Bearings Using Fractional Derivative Maxwell Model *Engineering Structures* **20(9)**, 849–856

4 KELLY, J M (1997) *Earthquake-Resistant Design with Rubber* New York Springer

5 KIKUCHI, M AND AIKEN I D (1997) An Analytical Hysteresis Model for Elastomeric Seismic Isolation Bearings *Earthquake Engineering and Structural Dynamics*, **26,** 215–231

6 KUESTER, J L AND MIZE, J H (1973) *Optimization Techniques with Fortran* New York McGraw Hill Inc

7 LEE, K -S (2002) Seismic Behavior of Structures with Structural Dampers Made from Ultra High Damping Natural Rubber, Ph D Dissertation, Department of Civil and Environmental Engineering, Lehigh University

8 *MTS SYSTEM CORPORATION (1991) System* Information for 810 Material Test System, Vol **1** and **2**

9 MULLINS, L, HARWOOD, J A C, AND PAYNE, A R (1967) Stress Softening in Rubbers – A Review *J Instn Rubb Ind*, 1967, **1** 17–27

10 PAPOULIA, K-D, AND KELLY, J M (1990) Material Characterization of Elastomers Used in Earthquake Base Isolation Report No UCB/EERC-90/18, Earthquake Engineering Research Center, University of California at Berkeley, Berkeley, California

11 WEN, Y-K (1976) Method for Random Vibration of Hysteretic Systems *Journal of the Engineering Mechanics Division*, ASCE, **102**, 249–263